Analog Current-Mode CMOS Implementation of Central Pattern Generator for Robot Locomotion

Kazuki Nakada, Tetsuya Asai, Tetsuya Hirose, Yoshihito Amemiya

Department of Electrical and Engineering

Hokkaido University

Sapporo, 060-8628

E-mail: nakada@sapiens-ei.eng.hokudai.ac.jp

Abstract— **We propose an analog current-mode central pattern generator (CPG). Our circuit is based on the neural oscillator proposed by Matsuoka, well known as a building block for constructing a robot locomotion controller. We modified the Matsuoka's oscillator to be suitable for analog current-mode implementation, and implemented it as an analog integrated circuit with current-mode low-pass filters. The oscillator circuit operates in the subthreshold region under the low-supply voltages, and thus low power consumption can be expected. We constructed a CPG circuit with four oscillator circuits. Through SPICE simulations, we confirmed that the CPG circuit generates stable phase-locked oscillation corresponding to typical locomotion of patterns of animals, and that the amplitude and frequency of the oscillation can be controlled by tuning bias currents over a wide range.**

I. INTRODUCTION

Locomotor behavior of animals, such as walking, running, flying, and swimming, is generated by the central nervous system, called the central pattern generator (CPG) [1]. A CPG consists of sets of neural oscillators, situated in the ganglion or spinal cord. Induced by inputs from higher level, a CPG generates rhythmic neural activity activating muscles in the absence of sensory inputs, resulting in locomotor behavior of animals. While not necessary for generating rhythmic activity, sensory inputs regulate such rhythmic activity over a wide range [1]. As a result, CPG adapts locomotor behavior to unpredictable environments.

During the past decade, many researchers have utilized such adaptability of CPG to locomotion control in robotics [5]-[7]. Taga *et al.* have used a CPG model that consists of the neural oscillator model proposed by Matsuoka [3], in simulating for biped locomotion [5]. Kimura *et al.* developed a CPG-based controller for quadruped robot locomotion on rough terrain [7]. Williamson also developed a CPG-based controller for rhythmic arm movements [6]. Lewis and his colleagues developed and mounted CPG chips on biped walking robots [12]-[13]. In these works, sensory feedback plays a critical role to high adaptability of CPG-based locomotion control.

In previous works, many CPG chips have been developed [8]-[17]. As a CPG chip, it is desirable to control the frequency and amplitude of the oscillation in the CPG chip over a wide range because such controllability is necessary to utilize sensor feedback efficiently in adapting the oscillation generated by the CPG chip to a given environments.

The aim of this work is to implement an analog CPG circuit with high controllability of the amplitude and frequency of the oscillation. We designed an analog current-mode neural oscillator, which operates in the subthreshold region under the low-supply voltages, based on the neural oscillator model proposed by Matsuoka. We also constructed a CPG circuit from the neural oscillator circuits. As a result, the CPG circuit generates stable phase-locked oscillation, and the amplitude and frequency of the oscillation can be controlled by tuning bias currents over a wide range.

II. HALF-CENTER OSCILLATOR CIRCUIT

We proposed an analog current-mode circuit implementing a half-center oscillator oscillator as a building block for constructing a CPG circuit.

A. Half-center Oscillator Model

We here describe a half-center oscillator model for analog current-mode implementation. Brown proposed the concept of the half-center oscillator to account for the alternating rhythmic activity in the flexor and extensor motoneuron during walking in cat [2]. A half-center oscillator consists of two neurons, a flexor half-center and an extensor half-center, with reciprocal inhibition (Fig. 1). The half-centers alternatively activate flexor and extensor muscles in the absence of pacemaker cells. Each half-center has dynamic properties such as self-inhibition, fatigue or adaptation. The flexor half-center activates the flexor muscles and suppresses the extensor half-center via synaptic inhibition in the flexion phase, in turn, due to the self-inhibition and adaptation, transition from the flexion phase to extension phase occurs.

Matsuoka proposed a half-center oscillator model that consists of two-neurons, described by the following system equations [3]:

$$\tau_u \frac{du_i}{dt} = -u_i + s - \beta v_i - w_{ij} f(u_j) \tag{1}$$

$$\tau_v \frac{dv_i}{dt} = -v_i + f(u_i) \tag{2}$$

where the nonlinear function $f(x) = \max(0, x)$, u_i represents the inner state of the i-th neuron, v_i an adaptation variable of the neuron $(i = 1, 2)$, s a tonic input, w_{ij} a synaptic strength between the i-th and j-th neuron, β the adaptation
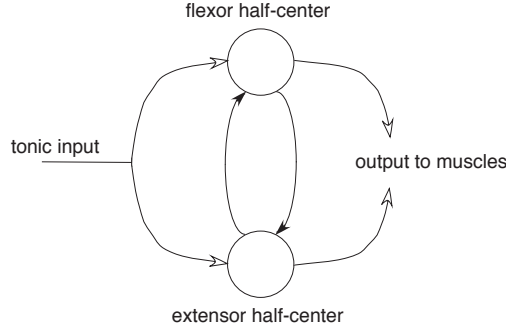
Fig. 1. Schematic of the half-center oscillator. Black and white arrows represent inhibitory and excitatory synapses.
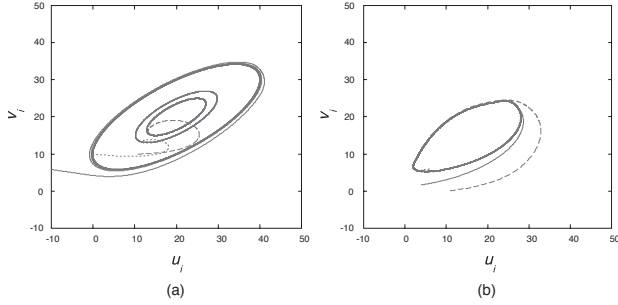

Fig. 2. Phase-plane portraits of (a) the Matsuoka model and (b) the proposed model. There exists multiple steady states for same parameter values in the Matsuoka model.

Fig. 3. Block diagram of the proposed model, where LPF represents a low-pass filter and f the nonlinear function.

Fig. 4. Schematic of current-mode low-pass filter.

effectiveness, τ_u a time constant of the self-inhibition, and τ_v a time constant of the adaptation effect.

This model generates limit-cycle oscillations depending on these parameters. The stability and properties of this model are analyzed in [3]-[4]. The amplitude of the oscillation is proportional to a tonic input, and the frequency and shape of the oscillation can be controlled by tuning the ratio of time constants. Utilizing such properties, this model has been fluently used in robotics [5]-[7]. Taga *et al.* have used it in simulating for biped locomotion. Williamson has applied it to control robot arm movements [6]. Kimura *et al.* applied it to control a quadruped robot on rough terrain [7].

Despite these advantages, a problem is that this model has multiple solutions for a same parameter set, as it is shown in Fig. 2. This occurs when we determine a parameter set to make all variables positive. To avoid this problem, we modified the Matsuoka model as follows:

$$\tau_u \frac{du_i}{dt} = -u_i + f(s - \beta v_i - w_{ij}u_j) \quad (3)$$

$$\tau_v \frac{dv_i}{dt} = -v_i + f(u_i) \quad (4)$$

where all variables and parameters are same as in (1)-(2). As a result, we can obtain a limit-cycle solution such that all variables are positive, and thus this model is suitable to implement as an analog current-mode circuit that uses uni-directional currents.
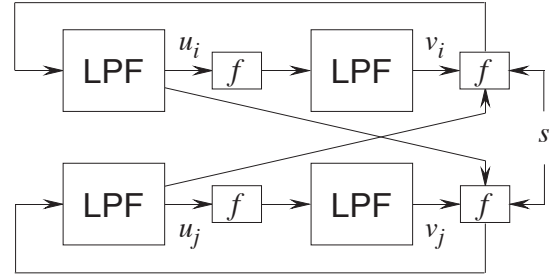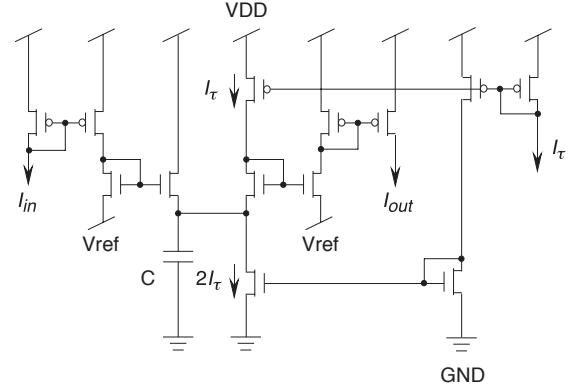
B. Circuit Architecture

We implemented the half-center oscillator model described in the previous section as an analog current-mode circuit.

The proposed model consists of four low-pass filters and nonlinear functions (Fig. 3). Thus, it can be implemented with current-mode low-pass filters and current mirrors. The current-mode low-pass filter (Fig. 4) operates in log-domain based on the dynamic translinear principle [18]. The circuit dynamics is expressed by the following equation:

$$\tau \frac{dI_{out}}{dt} = -I_{out} + I_{in} \quad (5)$$

where I_{in} is the input current, I_{out} the output current, and τ the time constant expressed by:

$$\tau = \frac{CU_T}{I_\tau} \quad (6)$$

where C the capacitance, U_T the thermal voltage, and I_τ the bias current. The nonlinear function defined by (3) can be easily implemented with current mirrors. We constructed a half-center oscillator circuit from current-mode low-pass filters and current mirrors, as shown in Fig. 5. The circuit dynamics is expressed by the following equations:

$$\tau \frac{dI_{u_i}}{dt} = -I_{u_i} + f(I_s - \beta I_{v_i} - wI_{u_j}) \quad (7)$$

$$\tau \frac{dI_{v_i}}{dt} = -I_{v_i} + f(I_{u_i}) \quad (8)$$

where I_{u_i} are the currents that corresponds to the inner state of the i-th neuron, I_{v_i} the currents that corresponds to
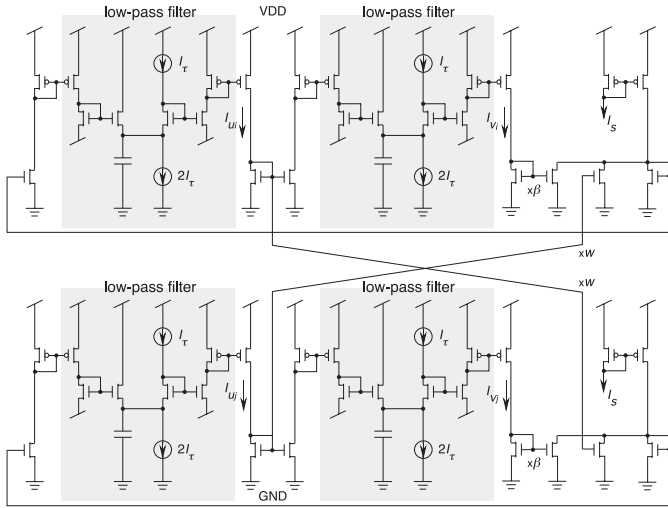
Fig. 5. Schematic of the oscillator circuit.

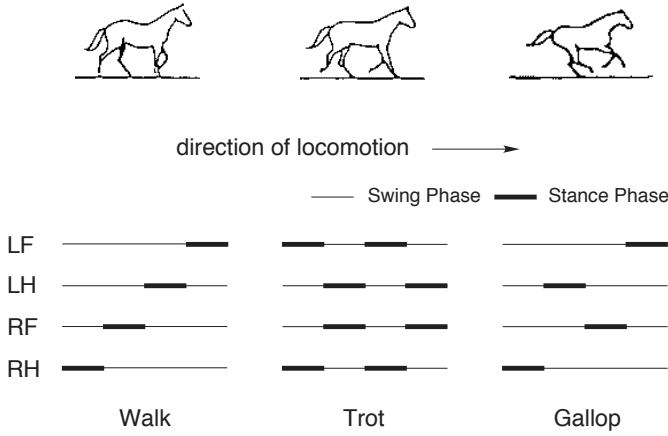direction of locomotion ⟶

—— Swing Phase ▬▬ Stance Phase

Fig. 6. Phase diagrams of typical locomotion patterns of mammals.

to an adaptation variable of the neuron, I_s the currents that corresponds to a tonic input, w_{ij} a synaptic strength between the i-th and j-th neuron, β the adaptation effectiveness, and τ a time constant. The parameters w_{ij} and β are determined by the aspect ratio of transistors comprising current mirrors. The time constant can be controlled by tuning the bias current I_τ. Depending on these circuit parameters, this circuit generates a stable limit-cycle oscillation.

III. CPG Circuit for Quadruped Locomotion

We here describe a CPG circuit for controlling interlimb coordination in quadruped locomotion.

In nature, animals show a wide variety of locomotion behaviors. For instance, horses show distinct locomotion patterns, such as walk, trot, and gallop. These patterns are characterized by phase relation ship in limb movements. In other words, these locomotion patterns are also considered as phase-locked oscillation of the limbs. Figure 6 shows phase diagrams of typical locomotion patterns of mammals like horses, where LF, LH, RF, and RH represent the left forelimb, left hindlimb,
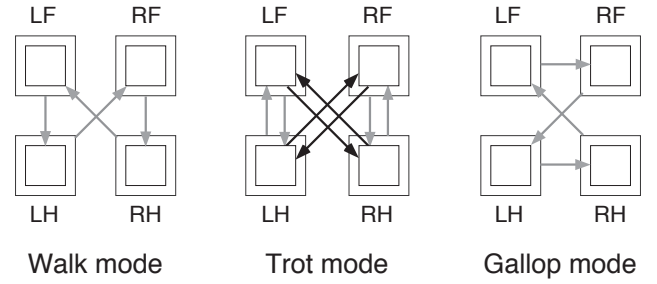

Fig. 7. Network configurations of CPG circuit.

right forelimb, and right forelimb, and bold and thin lines represent stance phases and swing phase during locomotion.

We constructed a CPG circuit from four half-center oscillator circuits. The CPG circuit generates phase-locked oscillation patterns corresponding to typical locomotion patterns of animals according to its network configurations (Fig. 7).

The circuit dynamics of the network circuit in walk mode are represented as follows:

$$\tau \frac{dI_{u_{\{1,2\}}}^{\mathrm{LF}}}{dt} = -I_{u_{\{1,2\}}}^{\mathrm{LF}} + f(I_{s,u_{\{1,2\}}}^{\mathrm{LF}} - \beta I_{v_{\{1,2\}}}^{\mathrm{LF}} - w I_{u_{\{2,1\}}}^{\mathrm{LF}}) \quad (9)$$

$$\tau \frac{dI_{u_{\{1,2\}}}^{\mathrm{LH}}}{dt} = -I_{u_{\{1,2\}}}^{\mathrm{LH}} + f(I_{s,u_{\{1,2\}}}^{\mathrm{LH}} - \beta I_{v_{\{1,2\}}}^{\mathrm{LH}} - w I_{u_{\{2,1\}}}^{\mathrm{LH}}) \quad (10)$$

$$\tau \frac{dI_{u_{\{1,2\}}}^{\mathrm{RF}}}{dt} = -I_{u_{\{1,2\}}}^{\mathrm{RF}} + f(I_{s,u_{\{1,2\}}}^{\mathrm{RF}} - \beta I_{v_{\{1,2\}}}^{\mathrm{RF}} - w I_{u_{\{2,1\}}}^{\mathrm{RF}}) \quad (11)$$

$$\tau \frac{dI_{u_{\{1,2\}}}^{\mathrm{RH}}}{dt} = -I_{u_{\{1,2\}}}^{\mathrm{RH}} + f(I_{s,u_{\{1,2\}}}^{\mathrm{RH}} - \beta I_{v_{\{1,2\}}}^{\mathrm{RH}} - w I_{u_{\{2,1\}}}^{\mathrm{RH}}) \quad (12)$$

$$\tau \frac{dI_{v_{\{1,2\}}}^{\mathrm{LF}}}{dt} = -I_{v_{\{1,2\}}}^{\mathrm{LF}} + f(I_{v_{\{1,2\}}}^{\mathrm{LF}})$$

$$\tau \frac{dI_{v_{\{1,2\}}}^{\mathrm{LH}}}{dt} = -I_{v_{\{1,2\}}}^{\mathrm{LH}} + f(I_{v_{\{1,2\}}}^{\mathrm{LH}}) \quad (13)$$

$$\tau \frac{dI_{v_{\{1,2\}}}^{\mathrm{RF}}}{dt} = -I_{v_{\{1,2\}}}^{\mathrm{RF}} + f(I_{v_{\{1,2\}}}^{\mathrm{RF}}) \quad (14)$$

$$\tau \frac{dI_{v_{\{1,2\}}}^{\mathrm{RH}}}{dt} = -I_{v_{\{1,2\}}}^{\mathrm{RH}} + f(I_{v_{\{1,2\}}}^{\mathrm{RH}}) \quad (15)$$

where $I_{u_i}^{\mathrm{LF,LH,RF,RH}}$ are the currents that correspond to the inner state of the i-th neuron at the joint of LF, LH, RF and RH, and $I_{v_i}^{\mathrm{LF,LH,RF,RH}}$ the currents that correspond to an adaptation variable of the neuron at the joint of LF, LH, RF, and RH. The currents I_{s,u_i}^{LF}, I_{s,u_i}^{LH}, I_{s,u_i}^{RF} and I_{s,u_i}^{RH} $(i = 1, 2)$ are represented as follows:

$$I_{s,u_{\{1,2\}}}^{\mathrm{LF}} = I_s + \gamma I_{u_{\{2,1\}}}^{\mathrm{RH}} \quad (16)$$

$$I_{s,u_{\{1,2\}}}^{\mathrm{LH}} = I_s + \gamma I_{u_{\{2,1\}}}^{\mathrm{LF}} \quad (17)$$

$$I_{s,u_{\{1,2\}}}^{\mathrm{RF}} = I_s + \gamma I_{u_{\{2,1\}}}^{\mathrm{LH}} \quad (18)$$

$$I_{s,u_{\{1,2\}}}^{\mathrm{RH}} = I_s + \gamma I_{u_{\{2,1\}}}^{\mathrm{RF}} \quad (19)$$

Fig. 8. Waveforms of currents of half-center oscillator circuit.

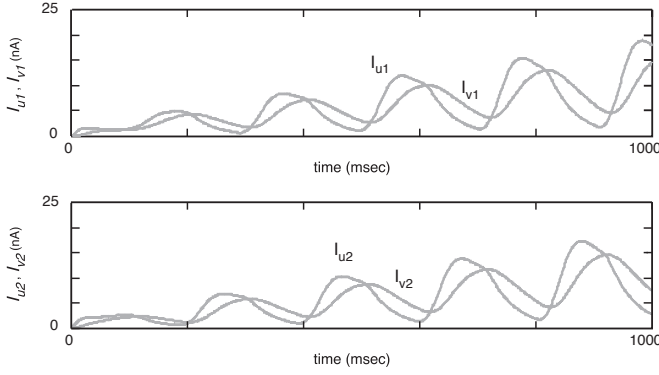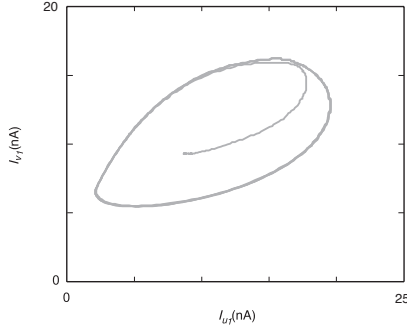Fig. 10. Amplitude modulation of waveforms of currents of half-center oscillator circuit.

Fig. 9. Phase-plane portrait of currents of half-center oscillator circuit.

Fig. 11. Frequency modulation of waveforms of currents of half-center oscillator circuit.

where I_s are the current that correspond to a tonic input, and γ a synaptic strength.

The circuit dynamics of the network circuit in trot mode are also represented by (9) - (12), where the currents I_{s,u_i}^{LF}, I_{s,u_i}^{LH}, I_{s,u_i}^{RF} and I_{s,u_i}^{RH} are represented as follows:

$$I_{s,u_{\{1,2\}}}^{\mathrm{LF}} = I_s + \gamma I_{u_{\{1,2\}}}^{\mathrm{RH}} + \gamma I_{u_{\{2,1\}}}^{\mathrm{LH}} \quad (20)$$

$$I_{s,u_{\{1,2\}}}^{\mathrm{LH}} = I_s + \gamma I_{u_{\{1,2\}}}^{\mathrm{RF}} + \gamma I_{u_{\{2,1\}}}^{\mathrm{LF}} \quad (21)$$

$$I_{s,u_{\{1,2\}}}^{\mathrm{RF}} = I_s + \gamma I_{u_{\{1,2\}}}^{\mathrm{LH}} + \gamma I_{u_{\{2,1\}}}^{\mathrm{RH}} \quad (22)$$

$$I_{s,u_{\{1,2\}}}^{\mathrm{RH}} = I_s + \gamma I_{u_{\{1,2\}}}^{\mathrm{LF}} + \gamma I_{u_{\{2,1\}}}^{\mathrm{RF}}, \quad (23)$$

and the circuit dynamics of the network circuit in gallop mode are also represented by (9) - (12), where the currents I_{s,u_i}^{LF}, I_{s,u_i}^{LH}, I_{s,u_i}^{RF} and I_{s,u_i}^{RH} are represented as follows:

$$I_{s,u_{\{1,2\}}}^{\mathrm{LF}} = I_s + \gamma I_{u_{\{2,1\}}}^{\mathrm{RH}} \quad (24)$$

$$I_{s,u_{\{1,2\}}}^{\mathrm{LH}} = I_s + \gamma I_{u_{\{2,1\}}}^{\mathrm{RF}} \quad (25)$$

$$I_{s,u_{\{1,2\}}}^{\mathrm{RF}} = I_s + \gamma I_{u_{\{2,1\}}}^{\mathrm{LF}} \quad (26)$$

$$I_{s,u_{\{1,2\}}}^{\mathrm{RH}} = I_s + \gamma I_{u_{\{2,1\}}}^{\mathrm{LH}}. \quad (27)$$

IV. SIMULATION RESULTS

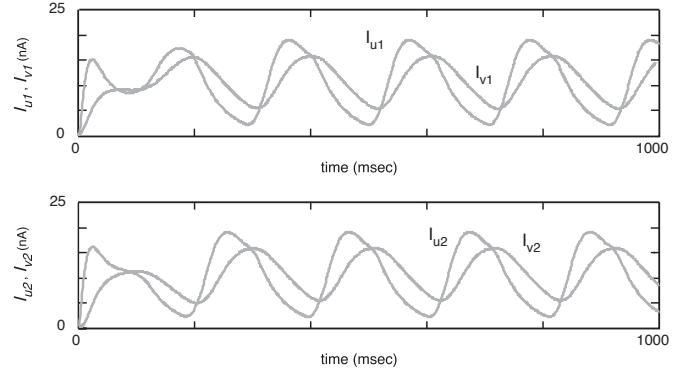We verified the operation of the half-center oscillator circuit and the CPG circuit with SPICE simulation. In the following simulations, we used MOSIS AMIS 1.5-μm LEVEL 49 model parameters. The gate length L of the transistor was set at L=9.6 μm, the gate width W of the minimum-size transistor was set at W=9.6 μm, the capacitance C=10 nF, and the supply voltages were set at VDD=1.5 V and Vref=0.35 V.

A. Half-center oscillator circuit

We here show the rhythmic pattern generation in the half-center oscillator circuit. Figure 8 shows the waveforms of the currents I_{u_i} and I_{v_i}, where the parameters β=5 and w_{ij}=4, and the bias currents were set at I_τ=10 nA and I_s=100 nA. The equilibrium currents of the circuit are calculated by solving the following equations:

$$\frac{dI_{u_i}}{dt} = \frac{dI_{v_i}}{dt} = 0, \quad (i = 1, 2) \quad (28)$$

that yield:

$$I_{u_o} = I_s - \beta I_{v_o} - w_{ij}I_{u_o}, \quad I_{v_o} = I_{u_o} \quad (29)$$

where I_{u_o} and I_{v_o} represent the equilibrium currents. Thus, the equilibrium currents become I_{u_o}=I_{v_o}=$I_s/10$. Figure 9 shows a closed (I_{u_i}, I_{v_i}) phase plane portrait. These results show the stable oscillation of the circuit.

The amplitude of the oscillation is proportional to the bias currents I_s because I_{u_i} and I_{v_i} are scaled by I_s. We changed the amplitude of the oscillation by tuning the bias current I_s
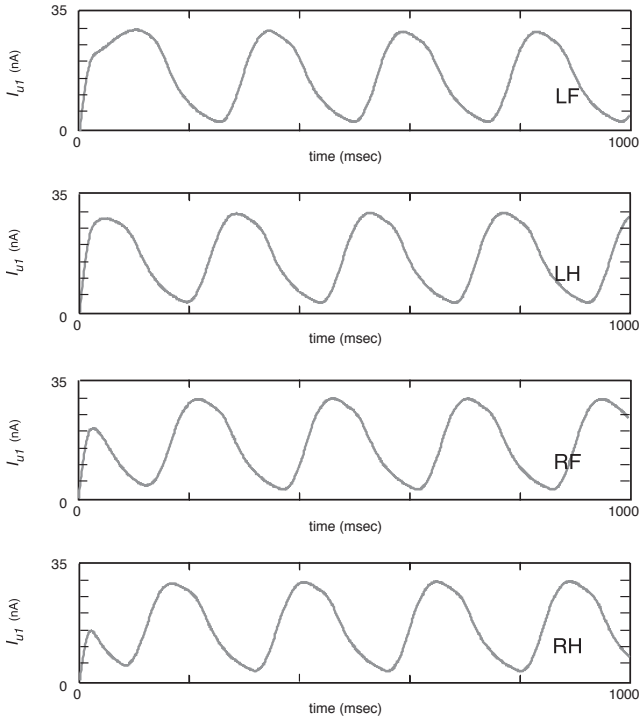
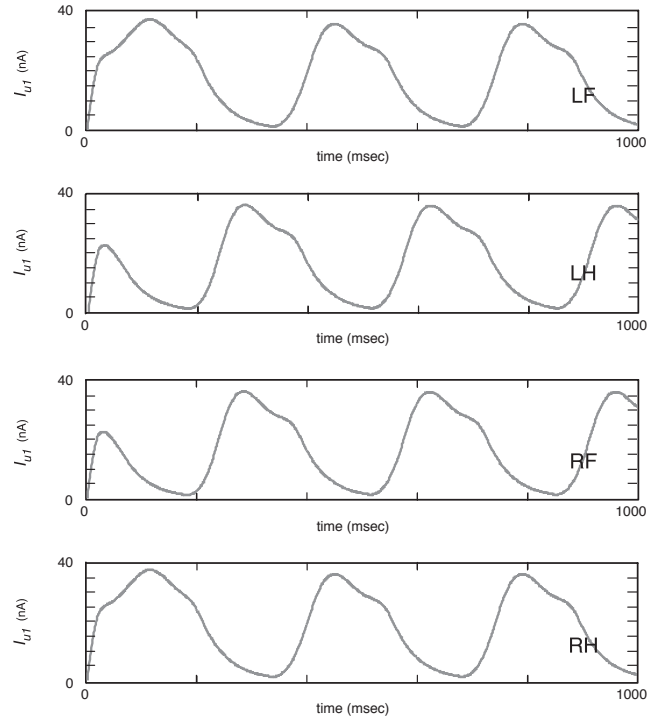Fig. 12. Waveforms of currents of CPG circuit operating in walk mode.

Fig. 13. Waveforms of currents of CPG circuit operating in trot mode.

from 10 nA to 100 nA as shown in Fig. 10. We also changed the frequency of the oscillation by tuning the bias current I_τ from 10 nA to 50 nA as shown in Fig. 11. These controllability of the amplitude and frequency of the oscillation are suitable for a building block for constructing a CPG controller.

B. CPG network circuit

We show the phase-locked oscillation in the CPG circuit. In the following simulations, we set the parameters $\beta=3$, $w_{ij}=3$, and $\gamma=0.33$. The synaptic strength γ are implemented with current mirrors as well as β and w. These parameters are fixed at the design stage. Figure 12 show the waveforms of the currents $I_{u_1}^{\mathrm{LF,LH,RF,RH}}$ of the CPG circuit operating in the walk mode. Figure 13 shows the waveforms of the currents $I_{u_1}^{\mathrm{LF,LH,RF,RH}}$ of the CPG circuit operating in the trot mode.

If we assumed that these curents give target joint angles to LF, RF, LH and RH of a robot, and then these phase-locked oscillation of the currents are considered as the typical locomotion patterns shown in Fig. 6.

We also show the amplitude modulation in the CPG circuit. When we decreased the bias current I_s of the half-center oscillator circuit for the individual joint RF from 100 nA to 75 nA at 2500 msec, the amplitude of the current $I_{u_1}^{\mathrm{RF}}$ was decreased. Figure 14 and 15 show the amplitude of the oscillation in the walk and trot mode, respectively.

These results show that the amplitude of the individual half-center oscillator circuit can be controlled independent of others. Such amplitude modulation is utilized to control quadruped robot locomotion.

V. CONCLUSIONS

We have designed an analog current-mode CMOS circuit for controlling interlimb coordination in quadruped robot locomotion. In previous works, many CPG circuits have been proposed [8]-[17]. As a CPG circuit, it is desirable to control the amplitude and frequency of the oscillation over a wide range. Hence, we have implemented the half-center oscillator model with high controllability of the amplitude and frequency of the oscillation as an analog current-mode circuit to use its controllability efficiently. The half-center oscillator circuit consists of four current-mode low-pass filters and several current mirrors. We have constructed a CPG circuit from four half-center oscillator circuits. The CPG circuit operates in subthreshold region under the low-supply voltages. Thus, low power consumption can be expected as well as previous current-mode neuromorphic chips [21].

Through SPICE simulations, we have shown that the CPG circuit generates stable phase-locked oscillation corresponding to the typical locomotion patterns of animals, and that the amplitude of the individual half-center oscillator circuit can be controlled independent of others. These characteristics of our circuit are suitable for controlling quadruped robot locomotion.

REFERENCES

[1] F. Delcomyn, *Foundations of Neurobiology*, New York: W. H. Freeman and Co., 1997.

[2] G. Brown, "On the nature of the fundamental activity of the nervous centers: together with an analysis of the conditioning of the rhythmic activity in progression, and a theory of the evolution of function in the nervous system," *J. Physiol.*, vol. 48, pp. 18-46, 1914.
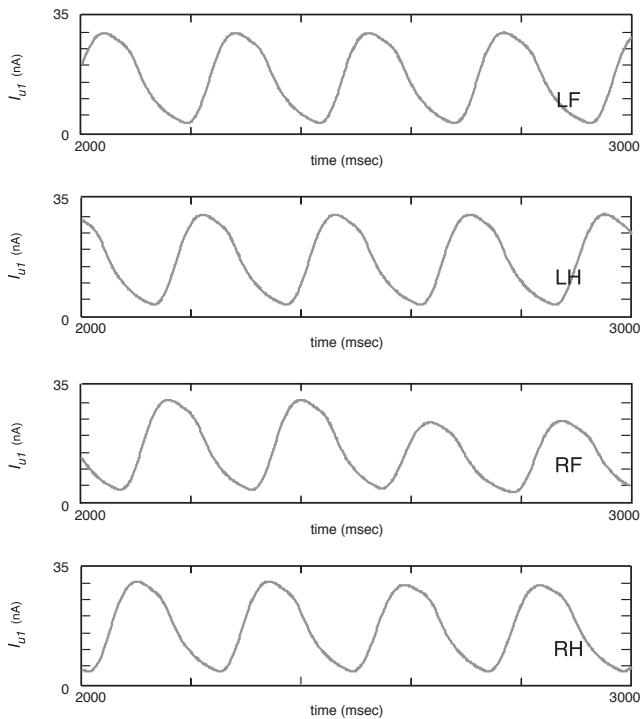
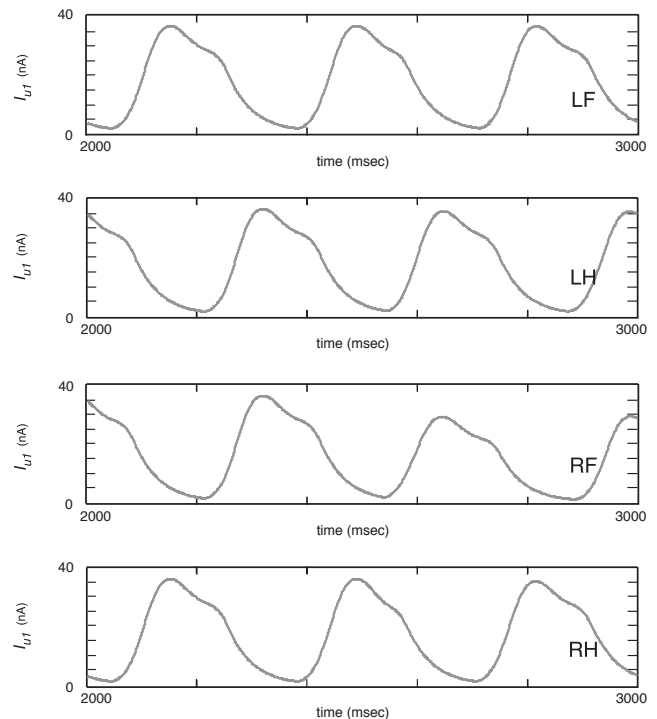Fig. 14. Amplitude modulation of CPG circuit operating in walk mode.

Fig. 15. Amplitude modulation of CPG circuit operating in trot mode.

[3] K. Matsuoka, "Sustained oscillations generated by mutually inhibiting neurons with adaptation." *Biol. Cybern.*, vol. 52, pp. 367-376, 1983.

[4] K. Matsuoka, "Mechanism of frequency and pattern control in the neural rhythm generators," *Biol. Cybern.*, vol. 56, pp. 345-353, 1987.

[5] G. Taga, Y. Yamaguchi and H. Shimizu, "Self-organaized control of bipedal locomotion by neural oscillators in unpredictable environment," *Biol. Cybern.*, vol. 65, pp.147-159, 1991.

[6] M. Wiiliamson, "Neural Control of Rhythmic Arm Movements" *Neural Networks, special issue on neural control of movement*, 1998.

[7] H. Kimura, Y. Fukuoka, and K. Konaga, "Adaptive dynamic walking of a quadruped robot by using neural system model", *ADVANCED ROBOTICS*, vol. 15, no. 8, pp. 859-876, 2001.

[8] S. Ryckebusch, J. M. Bower, C. A. Mead, "Modeling small oscillating biological networks in analog VLSI," *Adv. Neural Information processing Syst.*, vol. 1, pp. 384-393, 1989.

[9] S. Still. and M. W. Tilden, "Controller for a four legged walking machine," in *Neuromorphic Systems Engineering Silicon from Neurobiology*, Eds: L. S. Smith and A. Hamilton, World Scientific: Singapore, pp. 138-148, 1998.

[10] S. Still, B. Scholkopf, K. Hepp, R. J. Douglas, "Four-legged walking gait control using a neuromorphic chip interfaced to a support vector learning algorithm", *Adv. Neural Information processing Syst.*, vol. 13, pp. 741-747, 2001.

[11] G. Patel, J. Holleman, S. DeWeerth, "Analog VLSI model of inter-segmental cordination with nearest-neighbor coupling," *Adv. Neural Information processing Syst.*, vol. 10, pp. 710-725, 1998.

[12] M. A. Lewis, M. J. Harttmann, R. Etienne-Cummings, A. H. Cohen, "Control of a robot leg with an adaptive aVLSI CPG chip," *Neurocomputing*, vol. 38-40, pp. 1409-1421, 2001.

[13] F. Tenore, R. Etienne-Cummings, and M. A. Lewis, "A programmable array of silicon neurons for the control of legged locomotion," presented at *the International Symposium on Circuits and Systems*, Vancouver, 2004

[14] K. Nakada, T. Asai, and Y. Amemiya, "An analog central pattern generator for interlimb coordination in quadruped locomotion," *IEEE Trans. on Neural Networks*, vol. 14, no. 5, pp. 1356-1365, 2003.

[15] K. Nakada, T. Asai, and Y. Amemiya, "Analog CMOS implementation of a CNN-based locomotion controller with floating-gate devices," *IEEE Trans. Circuits and Syst. -I,* in press.

[16] M. Branciforte, G. Di Bernardo, F. Doddo, L. Occhipinti, "Reaction-Diffusion CNN design for a new class of biologically- inspired processors in artificial locomotion applications", in *Seventh International Conference on Microelectronics for Neural, Fuzzy and Bio-Inspired Systems*, pp. 69-77, Granada, Spain, 1999.

[17] P. Arena, S. Castorina, L. Fortuna, M. Frasca, M. Ruta, "A CNN chip for robot locomotion control", in *Proc. IEEE Int. Symp. Circuits Systems*, vol. 3, May 2003, pp. 510-513.

[18] J. Mulder, A. C. van der Woerd, W. A. Serdijn, H. M. van Roermund, "General current-mode analysis method for translinear filters," *IEEE Tran. Circuits and Syst. -I*, vol. 44, pp. 193-197, 1997.

[19] A. McEwan and A. van Schaik "A silicon representation of the meddis inner hair cell model," in *Proc. the ICSC Symposia on Intelligent Systems and Application*, paper 1544-078, 2000.

[20] W. Germanovix, C. Toumazou, "Design of a micropower current-mode log-domain analog cochlear implant", *IEEE Tran. Circuits and Syst. -II*, Vol. 47, No. 10, pp. 1023-1026, 2000.

[21] T. Serrano-Gotarredona and B. Linares-Barranco, "Log-domain implementation of complex dynamics reaction-diffusion neural networks", *IEEE Trans. on Neural Networks*, vol. 14, no. 5, pp. 1337-1355, 2003.